ACS NANO
Cite This: ACS Nano 2019, 13, 6867−6878
www.acsnano.org

ARTICLE

Nanotube-Mediated Path to Protocell Formation

Elif S. Köksal,[†] Susanne Liese,[‡] Ilayda Kantarci,[†] Ragni Olsson,[†] Andreas Carlson,[‡] and Irep Gözen*[,†,§,∥]

[†]Centre for Molecular Medicine Norway, Faculty of Medicine, University of Oslo, 0318 Oslo, Norway
[‡]Department of Chemistry, Faculty of Mathematics and Natural Sciences, University of Oslo, 0315 Oslo, Norway
[§]Department of Mathematics, Faculty of Mathematics and Natural Sciences, University of Oslo, 0315 Oslo, Norway
[∥]Department of Chemistry and Chemical Engineering, Chalmers University of Technology, SE-412 96 Göteborg, Sweden

Supporting Information

ABSTRACT: **Cellular compartments are membrane-enclosed, spatially distinct microenvironments that confine and protect biochemical reactions in the biological cell. On the early Earth, the autonomous formation of compartments is thought to have led to the encapsulation of nucleotides, thereby satisfying a starting condition for the emergence of life. Recently, surfaces have come into focus as potential platforms for the self-assembly of prebiotic compartments, as significantly enhanced vesicle formation was reported in the presence of solid interfaces. The detailed mechanism of such formation at the mesoscale is still under discussion. We report here on the spontaneous transformation of solid-surface-adhered lipid deposits to unilamellar membrane compartments through a straightforward sequence of topological changes, proceeding *via* a network of interconnected lipid nanotubes. We show that this transformation is entirely driven by surface-free energy minimization and does not require hydrolysis of organic molecules or external stimuli such as electrical currents or mechanical agitation. The vesicular structures take up and encapsulate their external environment during formation and can subsequently separate and migrate upon exposure to hydrodynamic flow. This may link the self-directed transition from weakly organized bioamphiphile assemblies on solid surfaces to protocells with secluded internal contents.**

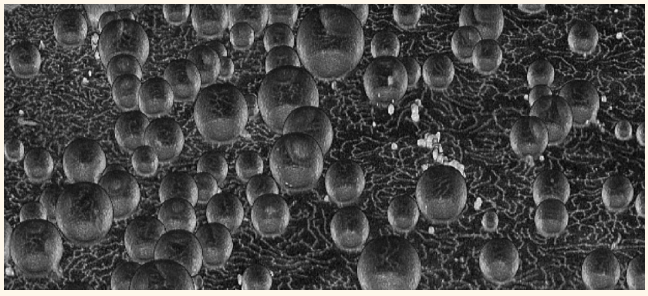

KEYWORDS: *protocell, biomembrane, lipid nanotube, origin of life, interface*

Topologically closed membranes are among the most conserved components of living systems. The earliest cell-like constructs were likely single amphiphile-membrane-enveloped aqueous microcontainers enclosing nucleotides.[1,2] In contemporary eukaryotic cells, multiple membrane compartments provide functionally specialized spaces that allow for localization and simultaneous operation of vital physiological processes that use common precursors. It has been argued that, with the ability of encapsulating nucleotides, maintaining them in physical proximity and empowering their replication by shielding them from random mixing, such compartmentalization, may have facilitated the first replication reactions, and thus were a critical enabling factor for the emergence of life.[2,3]

How compartments may have developed on the early Earth and what their exact structural and dynamic characteristics were is currently a subject of intense debate.[3−5] The first compartmentalization may have occurred with the self-assembly of previously disordered constitutive molecules as a result of specific, local interactions, without any distinct external stimuli. Among a variety of eligible molecular species, amphiphiles such as fatty acids or phospholipids are strong candidates, since they can self-organize to vesicular constructs. Because of their high critical micelle concentration (CMC) and high exchange rates, fatty acids are proposed more frequently as precursors for protocell formation as compared to phospholipids. However, the synthesis of some ubiquitous components of the biological membranes such as phosphatidic acid (PA), phosphatidyl etanolamine (PE), and phosphatidyl choline (PC) has been experimentally shown to also occur under primordial Earth conditions.[6−9] Primitive spherical compartments formed by self-assembled membranes share a number of characteristic features with biological cells, whose plasma membrane is also primarily composed of phospholipids. Among them are structural flexibility, wide size

Received: February 28, 2019
Accepted: June 8, 2019
Published: June 8, 2019

DOI: 10.1021/acsnano.9b01646
ACS Nano 2019, 13, 6867−6878

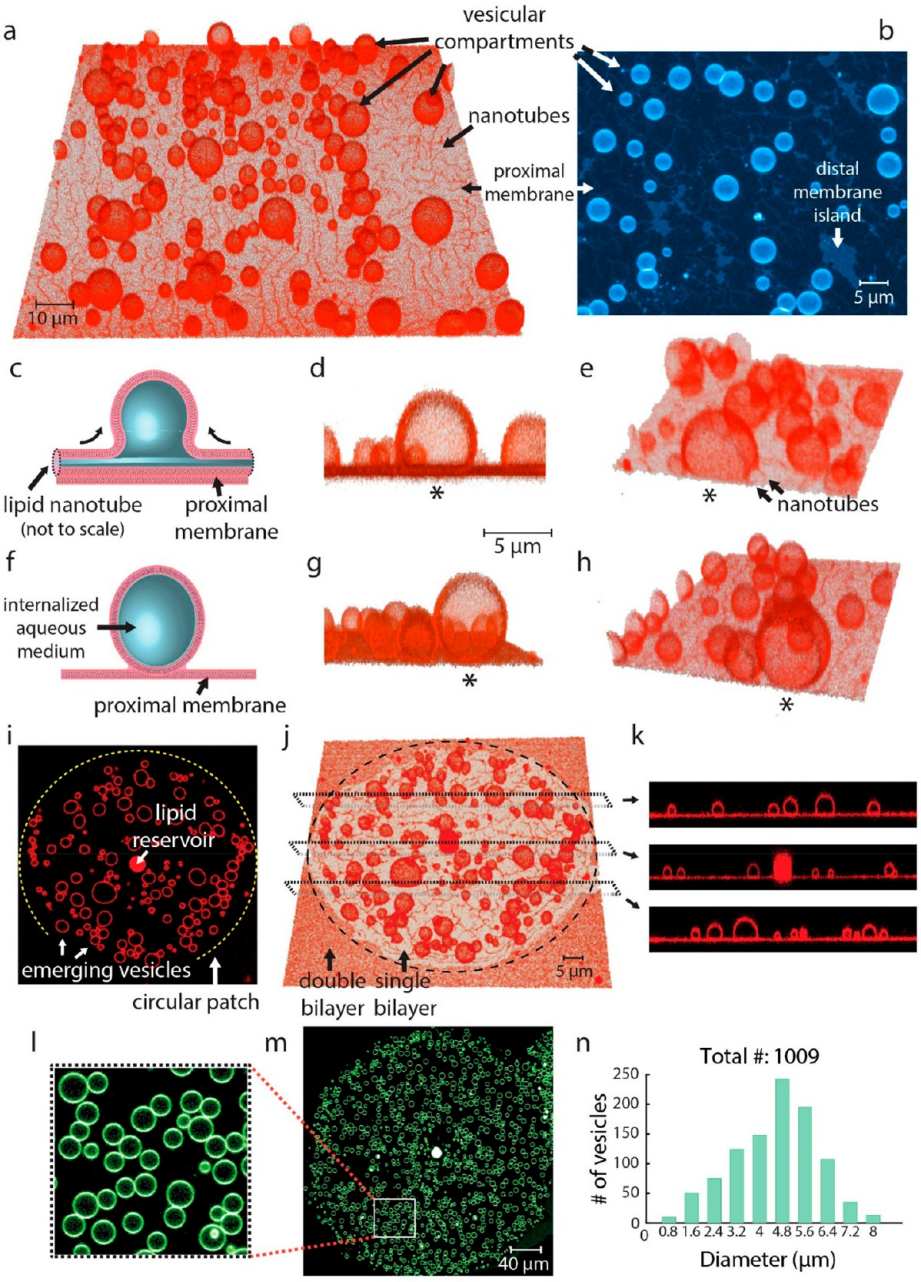

Figure 1. Giant vesicular compartment formation from surface-adhered lipid nanotubes. (a, b) Confocal micrographs, reconstructed in 3D, showing supported vesicles from (a) tilted view and (b) top view. Vesicles emerge from lipid nanotubes, which spontaneously form during dewetting of the proximal (lower) bilayer by the distal (upper) bilayer of an initially intact double-bilayer membrane. (c–e) Semigrown and (f–h) fully grown vesicular compartments. The vesicles, most of which are pinned to the proximal membrane *via* nanotubes, adopt a dome-shape (c–e). The connection of the vesicle to nanotubes is captured in (e). Over time, compartments mature to a spherical form (f–h). Vesicles, which are identical in (d, e) and (g, h), respectively, are marked with an asterisk. (i–k) Confocal micrographs of a circular membrane patch accommodating several vesicles: (i) top view (x–y plane), (j) tilted 3D view (x–y–z plane), (k) side views (x–z plane). The three separate profiles depicted in (k) correspond to the regions in (j) marked with dashed lines. The circular patch, as described in the main text in detail, is a result of self-spreading of a multilamellar lipid reservoir. The double-bilayer membrane of the adjacent reservoirs has spread around the ruptured patch in (j) (arrows showing single *vs* double bilayer). (l, m) Fluorescence micrograph of vesicles emerging from a circular patch, imaged in the x–y plane. In (l), the region in (m) framed with a white line is magnified. (n) Graph showing the number of vesicles in the membrane patch in (m) *versus* vesicle diameter. The patch contains over a thousand vesicles in total.

distribution, selective and tunable permeability, and the ability for growth and division and uptake and encapsulation of chemical reactants.

Most of the existing hypotheses on the formation of original biocompartments focus on bulk aqueous environments,[3,10] where a few are concentrating on assembly on solid surfaces, such as pyrites or clays.[3,4,11,12] The contact with surfaces would help reduce the energy barrier required for the assembly and enable the catalysis of chemical reactions. Under prebiotic conditions, organic molecules are thought to have self-assembled on inorganic solid surfaces, forming soft proto-biofilms,[4] although it is argued that the strong association

DOI: 10.1021/acsnano.9b01646
ACS Nano 2019, 13, 6867–6878

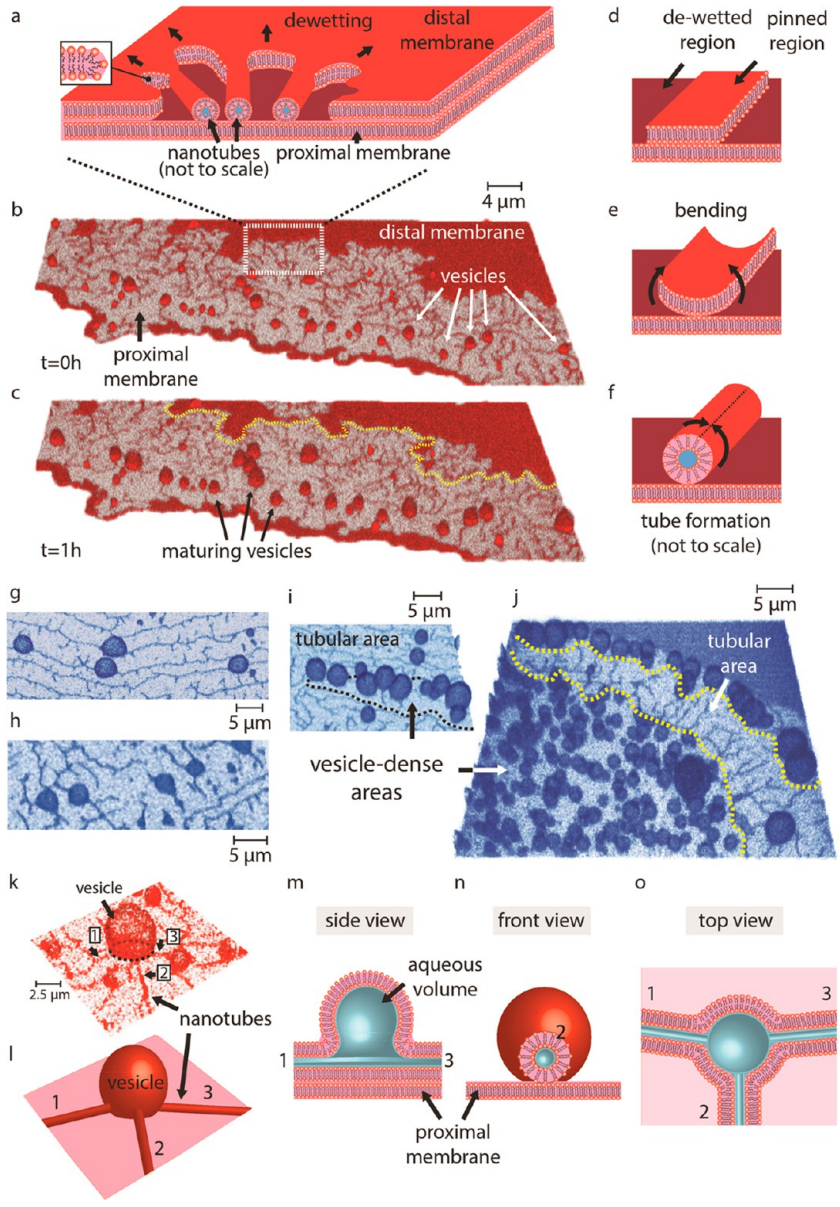

Figure 2. Formation of nanotubes and vesicles. (a) Spontaneous formation of lipid nanotubes during dewetting. Schematic representation of retraction of the distal membrane (red) over the proximal membrane (burgundy), leaving behind lipid threads. The confocal micrographs showing the corresponding experimental process are depicted in (b, c). The yellow, dashed line in (c) represents the contour of the distal membrane in (b). Initially, the parts of the distal membrane that are pinned to the proximal one remain (d). Such thin threads growing in length as the dewetting continues create increasing edge tension, which favors bending (e) followed by the nanotube formation (f). The nanotubes are not drawn to scale as the diameter of a lipid nanotube is 100−200 nm. In the cartoons, the membrane edge is shown as open. In reality, the membrane edge is curved (inset in (a)), to avoid the exposure of hydrophobic moieties of the membrane lipids to the aqueous buffer. The vesicles emerging from the nanotubes in (b) have grown larger in (c). (g, h) Emerging vesicular buds on lipid nanotubes. The vesicles appear spherical in the middle and elongated on the sides, where they connect to the nanotubes. (i, j) The areas populated by vesicles (regions framed in dashed lines) contain relatively less or no tubes. (k) The confocal image, reconstructed in 3D, and (l) the corresponding schematic representation of a vesicle emerging from/connected to multiple lipid nanotubes (numbered). (m−o) Schematic drawings explaining the configuration of the vesicle and nanotubes from different views.

constants that make the membrane adsorption on solid interfaces favorable would then prevent the detachment of the assembly.[3] In fact, Szostak and co-workers have made an important step forward when they showed enhanced vesicle formation upon adsorption of sheets of amphiphiles on various types of surfaces including the minerals.[3,11,12] The exact details of this formation process at the mesoscale remain to be elucidated.

Here we report on the spontaneous, stepwise transformation of surface-adsorbed lipid deposits into vesicular compartments. The deposits, which are giant multilamellar lipid reservoirs, undergo topological changes, sequentially adopting the forms of 2D molecular lipid films, then toroidal lipid nanotubes, and finally consistently unilamellar giant compartments. The transformation is driven by surface-free energy minimization and does not require energy-providing chemical transformations, *e.g.*, the hydrolysis of organic molecules, or external

DOI: 10.1021/acsnano.9b01646
ACS Nano 2019, 13, 6867−6878

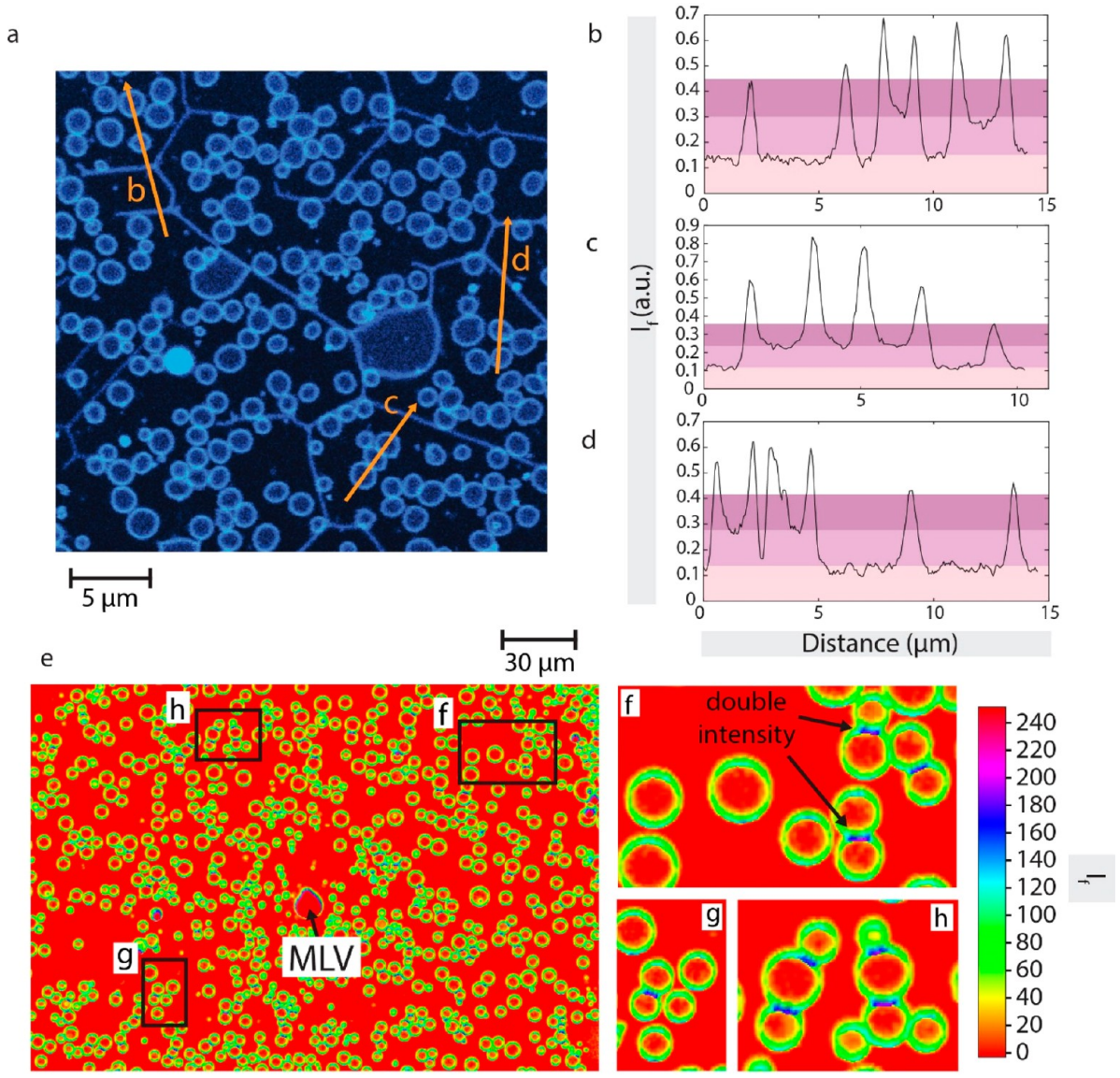

Figure 3. Lamellarity analysis. (a) Confocal fluorescence micrograph of a membrane region in the *x*−*y* plane. (b−d) Fluorescence intensity profiles along the orange lines in (a). The arrows indicate, from left to right, the direction of the profiles in panels (b−d). The intensities across the proximal membrane (single bilayer), the equator of the vesicle (two bilayers), and the nanotube (three bilayers) appear in a 1:2:3 ratio. (e) The false-colored fluorescence intensity plot of a membrane region containing over 100 vesicles shows nearly identical intensity (single lamellarity). (f−h) Close-ups of three different regions from (e). The overlapping membranes, where adjacent vesicles come in contact, have twice the intensity of the nonoverlapping regions, indicating single- and double-bilayer structures.

physical stimuli such as electrical currents or mechanical agitation. We show that the compartments encapsulate and hold a part of the medium they are created in and can separate from the surface and migrate under the influence of hydrodynamic forces.

The observed phenomena provide strong evidence that the transition from molecular amphiphile films on solid surfaces to spherical protocell compartments can occur spontaneously in simple aqueous environments in a materials-properties-driven, rather than a chemically initiated, process.

RESULTS/DISCUSSIONS

Spontaneous Emergence of Giant Vesicular Compartments from Surface-Adhered Lipid Nanotubes. We start the experiments by placing lipid reservoirs (multilamellar vesicles, MLVs) onto a SiO_2 substrate, which results in self-spreading of each reservoir on the solid support as a circular double-bilayer membrane.[13,14] Minutes after the MLV deposition, due to the continuous adhesion of the circular membrane's periphery to the solid substrate, the membrane tension reaches lysis tension (5−10 mN/m), leading to rupturing.[14] On the ruptured lipid patches, we observe the formation of numerous (100−1000 per patch) giant vesicular compartments, originating from surface-adhered phospholipid nanotubes (Figure 1a,b). The tubes, the formation of which is described in detail in subsequent paragraphs, appear during the retraction of the distal (upper) bilayer off the proximal (lower) bilayer of a double-bilayer membrane. The retracting upper membrane leaves behind a network of randomly pinned lipid nanoconduits on the proximal bilayer (Figure 1a). Islands of remaining distal membrane can be observed in Figure 1b. The vesicles emerge from the nanotubes, initially adopting a dome-

DOI: 10.1021/acsnano.9b01646
ACS Nano 2019, 13, 6867−6878

shape (Figure 1c−e) and, over time, a spherical giant unilamellar vesicle (GUV) (Figure 1f−h). The buds ($d \geq 0.8$ μm, Movies S1 and S2) appear within minutes and mature over a few hours to larger vesicles with diameters of 5−10 μm. During vesicle growth, the nanotubes are connected to the vesicles on one end and on the other end to the proximal bilayer (Figure 1e).

When an initially circular double membrane ruptures and transforms into a single bilayer, the circular contour is largely maintained. The vesicles therefore are concentrated in circular regions, with MLVs in the center (Figure 1i−k). Such vesicles, emerging from a ruptured circular patch, are shown in Figure 1i and j from different angles. In Figure 1k, three sections from panel j (frames in dashed lines) have been shown from the profile view. Except for the MLV, the vesicles appear to be unilamellar. If MLVs are added in high numbers to increase the membrane coverage of the surface, occasionally, the spreading double-bilayer membrane of adjacent reservoirs can spread around a ruptured single bilayer patch, as shown in Figure 1j.

A large lipid patch (d = ~300 μm) can accommodate about a thousand unilamellar vesicles (Figure 1l−n). The vesicle sizes vary from 1 to 10 μm in diameter, most in the range of 4−6 μm.

Formation of Nanotubes and Vesicles. During the rupturing described above, the distal membrane continuously dewets the proximal, leaving behind nanotube threads (Figure 2a−c). While the edge of the bilayer is shown open in the schematic drawings, in reality it is closed (inset Figure 2a), resulting in an increasing edge energy cost.[15,16] The dewetting process at a peripheral region of a lipid patch, leading to the formation of nanotubes and vesicles, is depicted in Figure 2b,c and Movie S3 (*cf.* Movies S4 and S5 for additional movies of growth). The contour of the edge of the retracting double-bilayer membrane in Figure 2b is superimposed on Figure 2c (yellow dashed line). Pinning among bilayers or between the bilayer and the solid substrate is mediated by the Ca^{2+} in the ambient buffer.[13,14,17] The elongation of the edges of the pinned threads due to continuous retraction of the distal bilayer causes an increase in edge tension, which eventually must lead to bending and toroidal tube formation (Figure 2d−f). Small buds appear on these tubes, which form and reside on the proximal membrane (Figure 2g,h). The buds initially adopt a semispherical or dome-like shape with elongated sides that are connecting to the nanotubes. These semispherical buds develop into spheres over time. It can be seen that the regions that are saturated with vesicles have a reduced nanotube density (Figure 2i,j), indicating that the tubes are consumed during vesiculation.

The vesicular compartments occasionally appear at the junction of several nanotubes. The confocal micrograph of a vesicle connected to at least three tubes (numbered) is shown in Figure 2k, and the corresponding schematic representations in Figure 2l−o. Figure 2m shows the profile view along nanotube #1−the vesicle−nanotube #3. In Figure 2n, nanotube #2 is elongating perpendicular to the plane of the page. The vesicle appears behind the cross-sectional view of the tube. Figure 2o is a top view of the vesicle and the three tubes with the proximal bilayer underneath (light pink color).

Consistent Unilamellarity. Because of the formation mechanism, the vesicles originating from a single bilayer appear consistently unilamellar. A confocal micrograph of a membrane region capturing several small vesicles and nanotubes on a proximal bilayer is shown in Figure 3a. The plots in Figure 3b−d show the fluorescence intensity profiles along the orange arrows in Figure 3a in indicated directions (for an additional number of analysis *cf.* Figure S1). The focal depth (x−z) of the confocal image shown in the x−y plane is ~1 μm. This means the micrograph of a vesicle on the surface with a diameter of ~2 μm captures the fluorescence signal starting from the solid substrate until only 1 μm above, which corresponds to approximately half of the spherical vesicle. For a 5 nm thick proximal bilayer and the lipid nanotubes (d = 100−200 nm), the fluorescence signal of the entire structure can be collected in the x−z direction. Accordingly, the intensities across the proximal membrane (single bilayer), the equator of the vesicles (two bilayers), and the nanotubes (three bilayers) appear in a 1:2:3 ratio (Figure 3b−d). To complement the analysis in Figure 3a−d and to verify the consistent lamellarity of multiple vesicles, a false-colored confocal image of a membrane area containing several vesicles is shown in Figure 3e−h. The z-axis of the scan is divided into intensity levels of an 8bit image (255 levels). The emission from labeled membranes of more than a hundred vesicles has nearly identical intensity (single bilayer) represented by the green color (Figure 3e). The regions between adjacent vesicles with overlapping bilayers appear as blue (*cf.* false color intensity scale), corresponding to the double intensity of a double-bilayer structure (Figure 3f−h).

Numerical Simulations of Vesicle Nucleation. In order to determine the relationships between the membrane area, its membrane bending energy, and the distance between two pinning points, we carried out finite element simulations (Figure 4), using the software Surface Evolver (SI). The pinning sites, or membrane defects, are assumed to be immobile points along the tube (Figure 4a) (*cf.* discussion). The ratio of the distance between the two closest pinning points (l) and the tube radius (r) gives the dimensionless number $k = \frac{l}{r}$, which is varied systematically in the simulations. In each simulation for a given k, a fixed membrane area $A > A_{\text{cylinder}}$ was defined, and the membrane area was allowed to equilibrate to a shape that corresponds to a minimum in bending energy E. In order to normalize the results for different distances between pinning defects, E and A were divided by their respective values for a cylindrical tube, with $E_{\text{cylinder}} = 2\pi k$ and $A_{\text{cylinder}} = 2\pi rl$. Figure 4a shows snapshots from the simulation of a nanotube evolving to a vesicle for k = 20. The model predicts the formation and growth of vesicles similar in size and shape to the ones observed experimentally (Figure 2g,h). Figure 4b shows the relation between the total energy and the surface area of the adhered tubes for different values of k. For $k \leq 15$ the energy exhibits a minimum; that is, the tube would have to overcome an energy barrier (energy of the highly curved neck region at either end of a bud) in order to transform into a spherical vesicle. In contrast, for longer tubes ($k \geq 20$) the energy decreases monotonically, which facilitates vesicle growth. Vesicle budding is initiated at $A/A_{\text{cylinder}} \geq 1$, where the total energy starts to deviate from the energy of a free-floating tube (solid black line). For large surface areas $A/A_{\text{cylinder}} > 6$, the energy approaches the value of a spherical vesicle (*cf.* SI). For each k value, the dashed lines in Figure 4b point to the magnitude of the total bending energy of spherical vesicles that are free of adhesion.

DOI: 10.1021/acsnano.9b01646
ACS Nano 2019, 13, 6867−6878

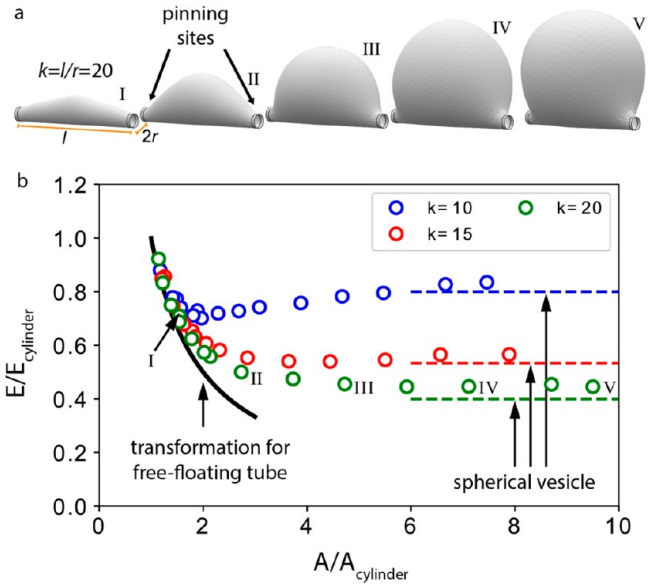

Figure 4. Bending energy *E* during tube−vesicle transformation. (a) Simulation snapshots showing the evolution of a nanotube to a vesicle, where the ratio *k* of the distance between two immobilized points along the tube (*l*) to tube radius (*r*) is 20. (b) Plots showing bending energy *vs* surface area of the adhered membrane structure (tube, bud, or vesicle) for three different values of *k*. For $k < 20$, indicating a short distance between the two fixed points (pinning sites), tube-to-vesicle transformation is unfavorable, while for $k \geq 20$, vesicle formation is favored. The energy values labeled I−V correspond to the vesicle shapes shown in (a). The corresponding dashed lines indicate the surface energy of completely spherical vesicles that are free of adhesion. The black solid line represents the transformation of a free-floating tube to a vesicle. Each simulation is repeated at least nine times for different initial conditions, and the variation in energy is within the size of the markers.

Encapsulation. Next, the supported bilayers were transformed in HEPES buffer containing fluorescein. Subsequently, the external solution was exchanged with HEPES buffer of identical composition and pH, but this time free of fluorescein (Figure 5a). The resulting vesicles encapsulated fluorescein in their internal volume and maintained it within. The cross section from the profile (x−z plane) of several vesicles is shown in Figure 5b. Figure 5c−r show confocal micrographs of four membrane regions from different lipid patches populated with vesicles encapsulating fluorescein and the corresponding intensity profiles. The vesicle membranes are labeled with rhodamine dye (red, Figure 5c,g,k,o), and the vesicles encapsulate 0.1 mM fluorescein (green, Figure 5d,h,l,p). Figure 5e,i,m,q show the rhodamine and the fluorescein channels superimposed. The fluorescence intensity profiles along the arrows in Figure 5e,i,m,q are shown in Figure 5f,j,n,r, respectively. In these plots, the vesicular membrane (plot in red color) appears as two close spikes, each corresponding to the bilayer membrane of the vesicle, and the fluorescein signal (plot in green color) remains in between the spikes, corresponding to the interior of the vesicle.

Separation and Migration of Vesicles. The GUVs that were initially anchored to the supported bilayer were exposed to hydrodynamic flow in the range of 10−100 nl/s by using the "multifunctional pipet", an open-space microfluidic device.[18,19] This exposure led to separation of the vesicles from the assembly (Figure 6). Briefly, the pipet injects a fluid stream into the vicinity of the vesicles through a central channel, while two peripheral channels simultaneously aspirate, creating a fluid recirculation zone within the existing medium (ambient buffer) without mixing the two (Figure 6a). The effective hydrodynamic flow in the exposure zone causes loosely surface-adhered objects to separate, and they can be collected in on-chip wells. By means of this setup, the surface-adhered vesicles were separated from the membrane patch, collected, and subsequently transferred with an automatic pipet onto gold-coated glass substrates in order to avoid rapid adhesion and rupturing, which typically occurs on glass slides. The vesicles adhering to the gold substrates are shown in Figure 6b and c (x−y−z plane). The inset to Figure 6c shows the top view (x−y) of vesicles #1−4. Figure 6d−g and h−j show two individual experiments capturing the separation and migration process. To be able to visualize the recirculation zone, fluorescein was used as tracer prior to the migration experiments (Figure 6d, dashed lines).

Our initial attempts of exposing the vesicles to several cycles of aspiration with the microfluidic pipet were resisted by the strong anchoring of the vesicles to the bilayer underneath (not shown). To be able to facilitate separation and collection, we weakened the pinning/anchor points of the vesicles. Accordingly, we exchanged the Ca^{2+}-containing ambient buffer with a Ca^{2+} chelator-containing solution. 1,2-Bis(*o*-aminophenoxy)ethane-*N*,*N*,*N*′,*N*′-tetraacetic acid (BAPTA) and ethylenediaminetetraacetic acid (EDTA)[18,20] were used in the experiments, and the vesicles with reduced pinning due to Ca^{2+} depletion were easily pulled into the pipet. During collection, some of the vesicles that were lifted by the aspiration force remain connected to the lipid patch through a nanotube (Figure 6d−g/Movie S6; 6h−j/Movie S7). Extrusion of nanotubes by exposing the vesicles to hydrodynamic flow is a well-characterized phenomenon.[21] All vesicles in regions 1−3 in Figure 6d−g and in regions 1 and 4 in Figure 6h−j separated and migrated toward the collection wells, while a few vesicles in regions 2 and 3 in Figure 6h−j remaining on the membrane after recirculation was terminated.

Tube Formation. During double-bilayer membrane rupturing, the distal membrane rapidly and continuously dewets the proximal membrane. The continuous wetting (adhesion of new membrane material to the surface) compensates for the increasing edge energy of the pore during rupture progression, while the proximal membrane is dewetted by the distal membrane. Eventually, the double-bilayer membrane fully transforms into a single-bilayer membrane. Throughout this process, some regions of distal membrane remain on the proximal membrane, owing to pinning. The distal membrane regions left behind during dewetting commonly appear in the form of tubular threads. A thread forms between the retracting membrane and a pinning site. Very rapidly, the edge energy $E_{edge} = \gamma l$, where γ is the line tension (5−10 pN) and l is the length of the elongating ruptured edge,[15,16] increases until the edges of the thread eventually bend, leading to toroidal tube formation. Figure 2d−f show one possible mechanism for nanotube formation, which assumes that the pinning creates a flat interface between the proximal and the distal bilayers. The lateral peripheries of a growing distal membrane thread rapidly bend upward and form a closed structure.

Pinning sites can form due to adhesion of two bilayers in close proximity caused by Ca^{2+} ions.[13,14,17,22−24] We also have trace amounts of Mg^{2+} ions present in the system (~10 μM) originating from the initial vesicle suspension. The binding

DOI: 10.1021/acsnano.9b01646
ACS Nano 2019, 13, 6867−6878

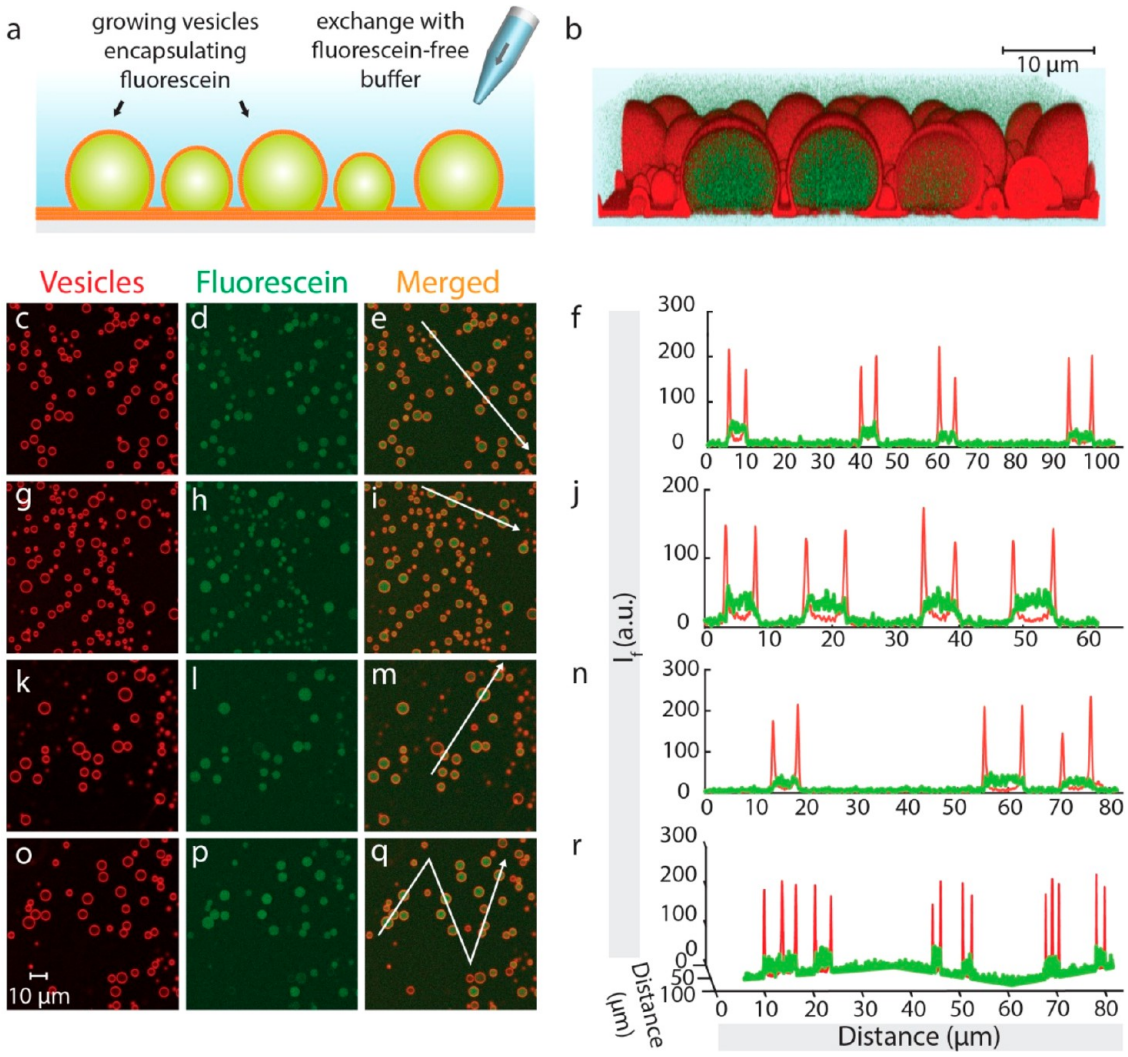

Figure 5. Encapsulation of fluorescein in vesicular compartments. (a) Schematic illustration and (b) confocal micrograph of vesicles encapsulating fluorescein (Fl), from a side view (x−z plane). Vesicles were grown in Fl-containing HEPES buffer. After maturation, the ambient solution was exchanged with Fl-free HEPES buffer, using an automatic pipet. (c−r) Fluorescence micrographs (x−y plane) and corresponding intensity profiles of vesicles encapsulating Fl. Panels c, g, k, o show membrane fluorescence, d, h, l, p the encapsulated Fl, and e, i, m, q combine both. The graphs in f, j, n, r show fluorescence intensity along the white arrows in e, i, m, q. The arrows indicate the direction of the depicted profiles from left to right. Red color represents the membrane fluorescence, and green color fluorescein.

efficiency of Ca^{2+} to lipid molecules is known to be higher than Mg^{2+}.[25] Even if Ca^{2+} and Mg^{2+} are present in similar concentrations, the interaction is dominated by Ca^{2+}. The pinning sites can also form dynamically due to rapid alterations in membrane tension.[26−28] The membrane patches we observe are large, with diameters of 300−400 μm. In such large areas, the membrane relaxation, for example due to a pore opening, cannot instantly propagate through the membrane evenly, but rather influences the membrane tension locally. Local membrane tension may indeed vary throughout our experiments, indicated by the simultaneous collapse and emergence of vesicles on the same membrane region (Figure S7). In our system the membrane locally experiences regions of strong and weak adhesion due to pinning and due to fluctuating membrane tension. The interaction of a membrane nanotube with a bilayer has been previously studied in great detail with dissipative particle dynamics (DPD) simulations,[26] which predict that strong adhesion leads to merging of the tube with the underlying bilayer membrane, whereas weak membrane adhesion promotes pearling.[26] Pearling instabilities can be observed when the local tension in the tube compared to the membrane material around it is high.[29,30] When excess membrane material becomes available in the membrane retraction process, the tube, in order to reduce its surface energy, transforms into a string of small spheres that are connected with very thin membrane necks.

Vesicle Formation and Growth Mechanism. The experimental evidence shows that the vesicles are formed *via* enlargement of the lipid nanotube fragments residing on a proximal bilayer (Figure 1 and Figure 2). Contraction of lengthy (l = 100 μm) lipid nanotubes to giant vesicles in short time scales (seconds to minutes) requires significant flip-flop rates, as well as rapid influx of ambient buffer. While high flip-flop rates can be accommodated during rapid shape transformations in high-curvature systems such as nanotubes,[31] the fast influx of an aqueous solution to a vesicle is only possible through membranes with abnormally high permeability.[32] Contraction of free-floating nanotubes to vesicles in short time scales therefore result in stomatocyte-like vesicular structures containing folded double bilayers.[32] In our experiments, the

DOI: 10.1021/acsnano.9b01646
ACS Nano 2019, 13, 6867−6878

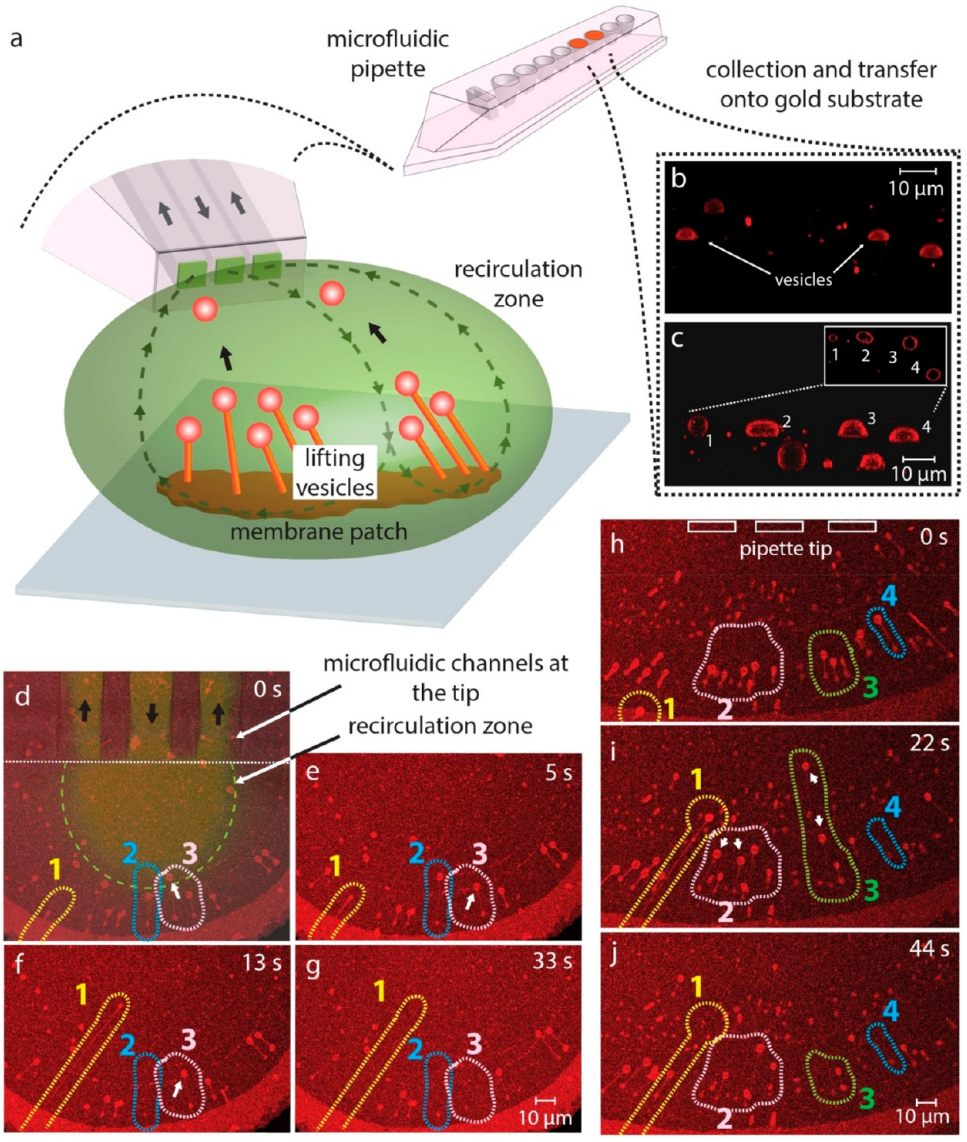

Figure 6. Separation and migration of vesicles after exposure to hydrodynamic forces. (a) Schematic illustration of the collection process, utilizing an open-space microfluidic device. The device circulates a liquid at its tip (green), by injecting from a central channel and aspirating simultaneously from the two peripheral channels. The objects in the ambient buffer entering into the recirculation zone separate from the membrane and migrate to collection wells, from which they can be retrieved. (b, c) Confocal florescence micrographs of the collected vesicles placed on gold substrates (x–y–z). Inset in (c) shows four of the vesicles in (c) (numbered) in the x–y plane. Fluorescein as tracer was used in (d) for better visualization of the recirculation zone (dashed line). (d–g and h–j) Separation of initially membrane-adhered vesicles from two different lipid patches. Transient nanotubes form while pulling the vesicles into the pipet. The vesicles in regions 1–3 in (d–g) and in region 1 and 4 in (h–j) were collected. A few vesicles in regions 2 and 3 in (h–j) remain on the membrane after recirculation is terminated.

nanotubes are pinned to the surface underneath. The pinning prevents rapid contractions, which would lead to the stomatocyte-like vesicles mentioned above. The formation of small buds in the micrometer range occurs within minutes, during which interleaflet lipid transfer might occur, whereas the maturation to giant vesicles takes hours to days, pointing to a simple mechanism of tube inflation in a low-membrane-tension regime.[33] Long time durations enable lateral lipid migration between the nanotube and the vesicular membrane. The lamellarity analyses shown in Figure 3 confirm that all of the resulting vesicle membranes are single bilayers, which indicates that the vesicles draw lipids from a remote single-bilayer source *via* a membranous connection, in contrast to the typical osmotically driven swelling processes of multilamellar reservoirs.

Source of Material for Vesicle Formation. The material consumed in the vesicle formation process can be efficiently supplied by the tubes. To form a vesicle with $d_{vesicle}$ = 5 μm, a nanotube (d_{tube} = 100 nm) with a length of 250 μm is required. This is well within the range of the tube lengths we are observing.[20] To fill the interior volume of this vesicle, however, solely from the internal aqueous volume of a toroidal lipid nanotube, the required tube length would be ~8 mm per vesicle. A significant portion of the aqueous volume inside the vesicles is therefore likely supplied from the ambient buffer through defects or transient pores in the vesicle membrane. Inflation of a toroidal nanotube by means of microinjection of

DOI: 10.1021/acsnano.9b01646
ACS Nano 2019, 13, 6867–6878

an aqueous medium through a membrane opening, resulting in a giant lipid container, has been reported earlier.[33,34] In these studies, the influx of 50×10^{-15} l/s of injected aqueous medium controlled by the micropipet was reported, corresponding to 10−60 $\mu m^2/s$ of membrane replacement.[33] Our observations, showing the spontaneous inflation of the tube to a 5 μm vesicle, indicate the influx to be as small as 2×10^{-18} l/s, which corresponds to a membrane replacement of 2×10^{-3} $\mu m^2/s$. This rate is well below the values observed for the micropipet injection method, supporting that the tube swelling/inflation as a mechanism for vesicle formation is realistic.

We observe that the entire vesicle population internalizes fluorescein (Figure 5). This further indicates that the internalization process involves primarily membrane openings, through which the external fluid can enter. This is an important detail, since the encapsulation of fluid can in other membrane systems[35] also proceed through osmotic pressure-induced swelling, where water molecules penetrate a bilayer membrane in order to relax an ion concentration gradient. The dehydration/rehydration procedure commonly utilized for vesicle fabrication is based upon the presence of dehydrated salt pockets, which produce osmotic stress, leading to water migration through the membrane and vesicle formation. In this case, larger molecules would not be internalizing along with water. While macromolecules could potentially also enter through the nanometer-size pores, their rate of internalization would be significantly smaller. On the other hand, synthesis of macromolecules might happen as well inside the vesicles, starting from small molecules. Since the compartments maintain integrity and hold the internalized contents, the pores must close after vesicle formation. It is likely that the permanent closure of the transient openings, possibly related to relaxation of membrane tension differences at late formation stages, terminates vesicle growth. We observe differences in fluorescence intensity in the vesicles, which we attribute to the presence of pores of different quantity and size in the membranes. This may be due to tension differences between the membranes of individual vesicles. Indeed, it has been reported[36] that the energy barrier for pore growth beyond a critical value in bilayer membranes decreases with increasing tension. At low tension (well below the lysis tension of 5 mN/m), pores that open during vesicle growth remain comparable to, or smaller than, the average size of the fluorescein molecule and would predominantly transfer water, while at higher tensions it is more likely that the pores become wide enough to transport fluorescein across the membrane. Pores must open and close continuously during vesicle growth, since the lifetime of a single microscale pore is only on the order of seconds,[15,37,38] and submicrometer pores on the order of nanoseconds.[39]

Driving Force for Tube-to-Vesicle Transformation. Lipid membrane nanotubes are highly curved. From the energy perspective, they are disfavored compared to spherical vesicles. By transforming a nanotube to a spherical vesicle, the curvature of the membrane is reduced and the surface free energy of the membrane is minimized.[40] Note that the surface free energy of a membrane is not exclusively defined by the bending energy, but it is the dominating term when high curvature is involved. When membrane material becomes available due to rupturing, the highly curved tube relaxes by incorporating the excess material, spontaneously transforming into the less curved, energetically more favorable spherical shape. The experimental observations (Figure 2g,h) and the predictions by the model (Figure 4) are in agreement. Vesicle formation is to a large extent driven by membrane curvature and bending energy minimization; both are materials-properties-related features and processes.

Location of Nucleation of the Vesicles. We currently do not know the factors that determine the locations of the nucleation sites. It is conceivable that the pinning sites, which are essential for tube formation, can also influence vesicle budding. One possible mechanism governing vesicle formation requires that pinning sites or membrane defects are also nucleation sites. Some vesicles are indeed connected by multiple tubes (Figure 2), which suggests that at least one pinning site is situated beneath the vesicle. Pearling instabilities in between two pinning sites, arising from a tension gradient between tube and surrounding membrane material, would provide a nucleation site, from which the vesicles can evolve. If we presume that the pinning points have a role in vesicle nucleation, through the numerical simulations we obtained the minimum distance of two points in between which a tube-to-vesicle transformation can occur. Bud formation initiates at $k = 20$ (Figure 4b); that is, for $d = 100$ nm the defects must be at least ∼1 μm apart from each other. This corresponds to the smallest vesicle sizes we observe (Figure 1n). Note that our model assumes that the vesicles nucleate in between two pinning sites. These sites, however, may not be necessarily physical boundaries of vesicle growth. Since number and density of the pinning sites are not exactly known, it cannot be excluded that vesicles incorporate several defects during growth.

Possible Implications for the Origins of Life. We show the spontaneous formation of consistently unilamellar lipid vesicles from surface-adhered phospholipid nanotubes. These spherical compartments possess an intact lipid bilayer and can engulf an aqueous volume containing solutes and organic compounds, both of which are essential features of a primitive protocell.[1,2] Compartmentalization is considered to be a fundamental step for the emergence of life, but how such containers were formed on the early Earth and what their exact structural and dynamic characteristics could be is currently the subject of an intense debate.[3,5] Under prebiotic conditions, structurally and functionally distinct organic molecules, in particular amphiphiles, are thought to have self-assembled on inorganic solid surfaces, forming soft proto-biofilms. The surfaces would assist the surfactants in overcoming the energetic barrier of self-assembling in a bulk aqueous solution without support.[4] Szostak and co-workers have reported facilitated vesicle formation in the presence of various types of solid particles including minerals[12] and proposed that the amphiphilic molecules were assembling into sheets close to the particle surface. The resulting vesicles were shown not to contain the fluorescently labeled layer adsorbed directly on the particles; that is, the vesicles were not physically stemming from the membrane directly in contact with the solid surface. How this enhanced formation occurred at the mesoscale is currently not known in detail, but the proposed models[3,12] support our findings that a second, distal bilayer forms the compartments. We also show that moderate hydrodynamic flow is able to separate and displace the vesicles from the surface, which could represent a primitive means of migratory mobility of intact protocells under reasonable ambient conditions.

DOI: 10.1021/acsnano.9b01646
ACS Nano 2019, 13, 6867−6878

CONCLUSIONS

We provide direct evidence showing a physical path of transformation from self-assembled amphiphile-based membranes on solid surfaces to spherical single-membrane compartments, proceeding *via* intermediate nanotubular structures. Very few assumptions have to be made to link this self-driven phenomenon directly to protocell formation. Strictly required are the presence of sufficient amphiphilic material, a high-energy solid surface, and suitable ambient conditions. We present strong evidence that due to the intrinsic physical and materials properties of the system, even without the need of agitation, sonication, and mechanical or hydrodynamic disturbance, nanotubes will spontaneously give rise to vesicular compartments. The suggested surface-assisted route to protocell formation also provides for alternative means of growth and division which, unlike the self-assembly in bulk solution, do not have to rely entirely on dynamic molecular properties of the involved amphiphilic species. Particularly relevant for the system we report here are earlier findings showing that upon mild agitation amphiphilic nanotubes form multiple daughter vesicles in a more efficient way, compared to the division of a large spherical vesicle into smaller vesicles.[8,41]

METHODS/EXPERIMENTAL

Stock Lipid Suspension. Various recipes of lipid mixtures were tested, a full list of which is provided in Table S1. To prepare each lipid composition, a dehydration and rehydration (gentle hydration) method described by Karlsson *et al.*[35] was followed. Briefly, lipids and lipid-conjugated fluorophores in designated ratios were mixed in chloroform, reaching a total concentration of 10 mg/mL. A 300 μL amount of this solution was placed in a 10 mL round-bottom flask, and the chloroform was removed in a rotary evaporator at reduced pressure (20 kPa) over a period of 6 h. The dry lipid film at the walls of the flask was rehydrated with 3 mL of phosphate-buffered saline (PBS) buffer containing 5 mM Trizma base, 30 mM K_3PO_4, 30 mM KH_2PO_4, 3 mM $MgSO_4{\cdot}7H_2O$, and 0.5 mM Na_2 EDTA, followed by addition of 3 μL glycerol. The pH of the PBS buffer was adjusted to 7.4 with H_3PO_4. The rehydrated lipid cake was kept at +4 °C overnight. In the final step, the lipid cake was sonicated for 10 s at room temperature to induce the formation of giant vesicles of varying, mainly multiple lamellarity.

Multilamellar Reservoir Formation. A 4 μL amount of each lipid suspension was placed on a coverslip and dehydrated in an evacuated desiccator for 20 min. The dry lipid film was rehydrated with ∼1 mL of HEPES buffer containing 10 mM HEPES and 100 mM NaCl (pH = 7.8, adjusted with NaOH) for 10 min to allow formation of MLVs. Then 100−200 μL of an MLV suspension was transferred onto an open-top observation chamber with SiO_2 substrate containing ∼1 mL of HEPES buffer with 10 mM HEPES, 100 mM NaCl, and 4 mM $CaCl_2$ (pH = 7.8, adjusted with NaOH), leading to spreading, rupturing, and formation of vesicles. The confluence of the MLVs on the surface can be adjusted by adding more or less MLV suspension, depending on the surface area and volume of the observation chamber. A 100−200 μL amount of MLV suspension in ∼1 mL of total volume gives moderate confluence for the rectangular chamber of 15 × 15 × 0.5 mm (1.125 cm^3 volume) used in the study.

Surface Fabrication and Characterization. SiO_2 deposited onto the glass substrates by reactive sputtering, using a MS 150 sputter system (FHR Anlagenbau GmbH) or e-beam and thermal PVD using EvoVac (Ångstrom Engineering), to final film thicknesses of 10 to 100 nm. The results were indifferent to film thickness. The thickness of the films was verified by ellipsometry (SD 2000 Philips). No precleaning was performed before deposition. Surfaces were stored at room temperature until use. Au films of 10 nm were deposited on glass coverslips on top of a 2 nm TiO_2, using the MS 150 sputter system.

Microscopy Imaging. A confocal laser scanning microscopy system (Leica SP8, Germany), with HCX PL APO CS 40× and 60× oil objectives and a 20× air objective, was used for acquisition of confocal fluorescence images. The utilized excitation/emission wavelengths for the imaging of the fluorophores were as follows: ex: 560 nm, em: 583 nm for rhodamine, ex: 488 nm, em: 515 nm for fluorescein, ex: 544 nm, em: 571 nm for TopFluor TMR. The results were indifferent to fluorophores.

Encapsulation. The main experiment the details of which were described above was reproduced in HEPES buffer containing 10 mM HEPES, 100 mM NaCl, 4 mM $CaCl_2$, and 100 μM fluorescein (NaFl salt, Sigma-Aldrich). After vesicle formation, the excess dye in the chamber was replaced by gently exchanging the Fl-containing HEPES buffer with the Fl-free HEPES using an automatic pipet.

Separation and Migration of GUVs. An open-volume microfluidic device/pipet (Fluicell AB, Sweden) was used to expose the initially surface-adhered vesicles to hydrodynamic flow, inducing their separation and migration. The pipet was positioned by a 3-axis water hydraulic micromanipulator (Narishige, Japan). The 10 mM HEPES buffer containing 100 mM NaCl, 10 mM EDTA, and 7 mM BAPTA (pH = 7.8, adjusted with NaOH) was used to weaken the Ca^{2+}-mediated adhesion of the vesicles to the underlying membrane. The vesicles were retrieved from the waste wells of the microfluidic device using an automatic pipet and placed on Au-coated glass surfaces.

Image Processing/Analysis. The 3D fluorescence micrographs were reconstructed using Leica Application Suite X (LasX) software (Leica Microsystems, Germany). Image enhancements to fluorescence micrographs were done with NIH Image-J software and Adobe Photoshop CS4 (Adobe Systems, USA). Schematic drawings and image overlays were created with Adobe Illustrator CS4 (Adobe Systems, USA). Vesicle counting and size distribution analyses were done using NIH Image-J software. Fluorescence intensity profiles were drawn in Matlab R2017a after applying median filtering. The false-colored fluorescence intensity plot was prepared with NIH Image-J Software Interactive 3D Surface Plot plugin.

Mathematical Model and Simulations. The minimal energy shapes of the budding tubes were determined with the finite element code Surface Evolver, an open-source software. Details are presented in the Supporting Information.

ASSOCIATED CONTENT

Supporting Information

The Supporting Information is available free of charge on the ACS Publications website at DOI: 10.1021/acsnano.9b01646.

Additional analyses of lamellarity; details of the mathematical model; images showing the collapse of the vesicles (alterations in membrane tension); tested lipid compositions; movies associated with the observed phenomena; data that support the findings of this study are available from the corresponding author upon reasonable request. (PDF)

Supporting movie 1 (AVI)

Supporting movie 2 (AVI)

Supporting movie 3 (AVI)

Supporting movie 4 (AVI)

Supporting movie 5 (AVI)

Supporting movie 6 (AVI)

Supporting movie 7 (AVI)

AUTHOR INFORMATION

Corresponding Author

*E-mail: irep@uio.no.

ORCID

Elif S. Köksal: 0000-0002-8921-3381

Irep Gözen: 0000-0002-5379-3273

DOI: 10.1021/acsnano.9b01646
ACS Nano 2019, 13, 6867−6878

Author Contributions

I.G. designed the research, E.K., I.K., R.O., S.L., and A.C. performed the research, E.K. analyzed the data, and E.K., S.L., A.C., and I.G. wrote the paper. An earlier version of this article has been posted on the preprint server bioRxiv.[42]

Notes

The authors declare no competing financial interest.

ACKNOWLEDGMENTS

We thank A. Jesorka from Chalmers University of Technology, Sweden, for technical advice, P. Dommersnes from the Norwegian University of Science and Technology, and T. Chan from the University of Oslo, Norway, for stimulating questions. This work was made possible through financial support obtained from the Research Council of Norway (Forskningsrådet) Project Grant 274433, UiO: Life Sciences Convergence Environment, the Swedish Research Council (Vetenskapsrådet) Project Grant 2015-04561, and the startup funding provided by the Centre for Molecular Medicine Norway (RCN 187615) & Faculty of Mathematics and Natural Sciences at the University of Oslo. S.L. and A.C. gratefully acknowledge funding from the Research Council of Norway Project Grant 263056.

REFERENCES

(1) Schrum, J. P.; Zhu, T. F.; Szostak, J. W. The Origins of Cellular Life. *Cold Spring Harbor Perspect. Biol.* **2010**, *2*, a002212.
(2) Szostak, J. W.; Bartel, D. P.; Luisi, P. L. Synthesizing Life. *Nature* **2001**, *409*, 387−390.
(3) Monnard, P. A.; Walde, P. Current Ideas about Prebiological Compartmentalization. *Life (Basel, Switz.)* **2015**, *5*, 1239−1263.
(4) Egel, R. Origins and Emergent Evolution of Life: The Colloid Microsphere Hypothesis Revisited. *Origins Life Evol. Biospheres* **2014**, *44*, 87−110.
(5) McNichol, J. Primordial Soup, Fool's Gold, and Spontaneous Generation: A Brief Introduction to the Theory, History, and Philosophy of the Search for the Origin of Life. *Biochem. Mol. Biol. Educ.* **2008**, *36*, 255−261.
(6) Rao, M.; Eichberg, J.; Oró, J. Synthesis of Phosphatidylethanolamine Under Possible Primitive Earth Conditions. *J. Mol. Evol.* **1987**, *25*, 1−6.
(7) Rao, M.; Eichberg, M. R.; Oro, J. Synthesis of Phosphatidylcholine Under Possible Primitive Earth Conditions. *J. Mol. Evol.* **1982**, *18*, 196−202.
(8) Budin, I.; Szostak, J. W. Physical Effects Underlying the Transition from Primitive to Modern Cell Membranes. *Proc. Natl. Acad. Sci. U. S. A.* **2011**, *108*, 5249−5254.
(9) Walde, P. Surfactant Assemblies and Their Various Possible Roles for the Origin(S) of Life. *Origins Life Evol. Biospheres* **2006**, *36*, 109−150.
(10) Terasawa, H.; Nishimura, K.; Suzuki, H.; Matsuura, T.; Yomo, T. Coupling of the Fusion and Budding of Giant Phospholipid Vesicles Containing Macromolecules. *Proc. Natl. Acad. Sci. U. S. A.* **2012**, *109*, 5942−5947.
(11) Hanczyc, M. M.; Fujikawa, S. M.; Szostak, J. W. Experimental Models of Primitive Cellular Compartments: Encapsulation, Growth. *Science (Washington, DC, U. S.)* **2003**, *302*, 618−622.
(12) Hanczyc, M. M.; Mansy, S. S.; Szostak, J. W. Mineral Surface Directed Membrane Assembly. *Origins Life Evol. Biospheres* **2007**, *37*, 67−82.
(13) Lobovkina, T.; Gözen, I.; Erkan, Y.; Olofsson, J.; Weber, S. G.; Orwar, O. Protrusive Growth and Periodic Contractile Motion in Surface-Adhered Vesicles Induced by Ca2+-Gradients. *Soft Matter* **2010**, *6*, 268−272.
(14) Gözen, I.; Dommersnes, P.; Czolkos, I.; Jesorka, A.; Lobovkina, T.; Orwar, O. Fractal Avalanche Ruptures in Biological Membranes. *Nat. Mater.* **2010**, *9*, 908−912.
(15) Karatekin, E.; Sandre, O.; Guitouni, H.; Borghi, N.; Puech, P. H.; Brochard-Wyart, F. Cascades of Transient Pores in Giant Vesicles: Line Tension and Transport. *Biophys. J.* **2003**, *84*, 1734−1749.
(16) Zhelev, D. V.; Needham, D. Tension-Stabilized Pores in Giant Vesicles: Determination of Pore Size and Pore Line Tension. *Biochim. Biophys. Acta, Biomembr.* **1993**, *1147*, 89−104.
(17) Akashi, K.-i.; Miyata, H.; Itoh, H.; Kinosita, K., Jr. Formation of Giant Liposomes Promoted by Divalent Cations: Critical Role of Electrostatic Repulsion. *Biophys. J.* **1998**, *74*, 2973−2982.
(18) Ainla, A.; Gözen, I.; Hakonen, B.; Jesorka, A. Lab on a Biomembrane: Rapid Prototyping and Manipulation of 2d Fluidic Lipid Bilayers Circuits. *Sci. Rep.* **2013**, *3* (3), 1−6.
(19) Ainla, A.; Jeffries, G. D. M.; Brune, R.; Orwar, O.; Jesorka, A. A Multifunctional Pipette. *Lab Chip* **2012**, *12*, 1255−1261.
(20) Bilal, T.; Gözen, I. Formation and Dynamics of Endoplasmic Reticulum-Like Lipid Nanotube Networks. *Biomater. Sci.* **2017**, *5*, 1256−1264.
(21) Borghi, N.; Kremer, S.; Askovic, V.; Brochard-Wyart, F. Tube Extrusion from Permeabilized Giant Vesicles. *Europhys. Lett.* **2006**, *75*, 666−672.
(22) Gozen, I.; Dommersnes, P.; Orwar, O.; Jesorka, A. Evidence for Membrane Flow through Pores in Stacked Phospholipid Membranes. *Soft Matter* **2012**, *8*, 6220−6225.
(23) Graber, Z. T.; Shi, Z.; Baumgart, T. Cations Induce Shape Remodeling of Negatively Charged Phospholipid Membranes. *Phys. Chem. Chem. Phys.* **2017**, *19*, 15285−15295.
(24) Feigenson, G. W. On the Nature of Calcium Ion Binding between Phosphatidylserine Lamellae. *Biochemistry* **1986**, *25*, 5819−5825.
(25) Mao, Y.; Du, Y.; Cang, X.; Wang, J.; Chen, Z.; Yang, H.; Jiang, H. Binding Competition to the Popg Lipid Bilayer of Ca2+, Mg2+, Na+, and K+ in Different Ion Mixtures and Biological Implication. *J. Phys. Chem. B* **2013**, *117*, 850−858.
(26) Yue, T.; Xu, Y.; Sun, M.; Zhang, X.; Huang, F. How Tubular Aggregates Interact with Biomembranes: Wrapping, Fusion and Pearling. *Phys. Chem. Chem. Phys.* **2016**, *18*, 1082−1091.
(27) Shillcock, J. C.; Lipowsky, R. Tension-Induced Fusion of Bilayer Membranes and Vesicles. *Nat. Mater.* **2005**, *4*, 225−228.
(28) Muller, M.; Katsov, K.; Schick, M. A New Mechanism of Model Membrane Fusion Determined from Monte Carlo Simulation. *Biophys. J.* **2003**, *85*, 1611−1623.
(29) Bar-Ziv, R.; Moses, E. Instability and "Pearling" States Produced in Tubular Membranes by Competition of Curvature and Tension. *Phys. Rev. Lett.* **1994**, *73*, 1392−1395.
(30) Liu, Y.; Agudo-Canalejo, J.; Grafmüller, A.; Dimova, R.; Lipowsky, R. Patterns of Flexible Nanotubes Formed by Liquid-Ordered and Liquid-Disordered Membranes. *ACS Nano* **2016**, *10*, 463−474.
(31) Raphael, R. M.; Waugh, R. E. Accelerated Interleaflet Transport of Phosphatidylcholine Molecules in Membranes under Deformation. *Biophys. J.* **1996**, *71*, 1374−1388.
(32) Stepanyants, N.; Zhang, H.; Lobovkina, T.; Dommersnes, P.; Jeffries, G. D. M.; Jesorka, A.; Orwar, O. Spontaneous Shape Transformation of Free-Floating Lipid Membrane Nanotubes. *Soft Matter* **2013**, *9*, 5155−5159.
(33) Karlsson, M.; Sott, K.; Cans, A. S.; Karlsson, A.; Karlsson, R.; Orwar, O. Micropipet-Assisted Formation of Microscopic Networks of Unilamellar Lipid Bilayer Nanotubes and Containers. *Langmuir* **2001**, *17*, 6754−6758.
(34) Jesorka, A.; Stepanyants, N.; Zhang, H.; Ortmen, B.; Hakonen, B.; Orwar, O. Generation of Phospholipid Vesicle-Nanotube Networks and Transport of Molecules Therein. *Nat. Protoc.* **2011**, *6*, 791−805.
(35) Karlsson, M.; Nolkrantz, K.; Davidson, M. J.; Strömberg, A.; Ryttsén, F.; Åkerman, B.; Orwar, O. Electroinjection of Colloid Particles and Biopolymers into Single Unilamellar Liposomes and

DOI: 10.1021/acsnano.9b01646
ACS Nano 2019, 13, 6867−6878

Cells for Bioanalytical Applications. *Anal. Chem.* **2000**, *72*, 5857−5862.
(36) Levadny, V.; Tsuboi, T.-a.; Belaya, M.; Yamazaki, M. Rate Constant of Tension-Induced Pore Formation in Lipid Membranes. *Langmuir* **2013**, *29*, 3848−3852.
(37) Karatekin, E.; Sandre, O.; Brochard-Wyart, F. Transient Pores in Vesicles. *Polym. Int.* **2003**, *52*, 486−493.
(38) Sandre, O.; Moreaux, L.; Brochard-Wyart, F. Dynamics of Transient Pores in Stretched Vesicles. *Proc. Natl. Acad. Sci. U. S. A.* **1999**, *96*, 10591−10596.
(39) Bennett, W. F. D.; Sapay, N.; Tieleman, D. P. Atomistic Simulations of Pore Formation and Closure in Lipid Bilayers. *Biophys. J.* **2014**, *106*, 210−219.
(40) Helfrich, W. Elastic Properties of Lipid Bilayers: Theory and Possible Experiments. *Z. Naturforsch., C: J. Biosci.* **1973**, *28*, 693−703.
(41) Zhu, T. F.; Szostak, J. W. Coupled Growth and Division of Model Protocell Membranes. *J. Am. Chem. Soc.* **2009**, *131*, 5705−5713.
(42) Köksal, E. S.; Liese, S.; Kantarci, I.; Olsson, R.; Carlson, A.; Gözen, I. A Nanotube-Mediated Path to Protocell Formation. 2018, 388405. *bioRxiv*. https://doi.org/10.1101/388405 (accessed August 17, 2018).

DOI: 10.1021/acsnano.9b01646
ACS Nano 2019, 13, 6867−6878